Liquefaction Mitigation of Silty Sands Using Rammed Aggregate Piers Based on Blast-Induced Liquefaction Testing

Published Version:
Rollins K.M., A.S. (2021). Liquefaction Mitigation of Silty Sands Using Rammed Aggregate Piers Based on Blast-Induced Liquefaction Testing. JOURNAL OF GEOTECHNICAL AND GEOENVIRONMENTAL ENGINEERING, 147(9), 1-16 [10.1061/(ASCE)GT.1943-5606.0002563].

Availability:
This version is available at: https://hdl.handle.net/11585/864235 since: 2022-02-22

Published:
DOI: http://doi.org/10.1061/(ASCE)GT.1943-5606.0002563

(Article begins on next page)

Liquefaction Mitigation of Silty Sands Using Rammed Aggregate Piers Based on Blast-Induced Liquefaction Testing.

Kyle M. Rollins[1], Sara Amoroso[2], Paul Andersen[3], Laura Tonni[4], Kord Wissmann[5]

Abstract: To investigate the liquefaction mitigation capability of Rammed Aggregate Piers® (RAP) in silty sand, blast liquefaction testing was performed at a soil profile treated with a full-scale RAP group relative to an untreated soil profile. The RAP group consisted of 16 piers in a 4x4 arrangement at 2 m center-to-center spacing extending to a depth of 9.5 m. Blasting around the untreated area induced liquefaction ($r_u \approx 1.0$) from 3 m to 11 m depth, producing several large sand boils, and causing settlement of 10 cm. In contrast, installation of the RAP group reduced excess pore water pressure ($r_u \approx 0.75$), eliminated sand ejecta, and reduced average settlement to between 2 to 5 cm when subjected to the same blast charges. Although the liquefaction-induced settlement in the untreated area could be accurately estimated using an integrated CPT-based settlement approach, settlement in the RAP treated area was significantly overestimated with the same approach even after considering RAP treatment-induced densification. Analyses indicate that settlement after RAP treatment could be successfully estimated from liquefaction-induced compression of the sand and RAP acting as a composite material. This test program identifies a mechanism that explains how settlement was reduced for the RAP group despite the elevated r_u values in the silty sands that are often difficult to improve with vibratory methods.

[1] Prof., Department of Civil and Environmental Engineering, Brigham Young University, 430 Engineering Building, Provo, UT 84602, ORCID: https://orcid.org/0000-0002-8977-6619X, email: rollinsk@byu.edu
[2] Assistant Prof., Department of Engineering and Geology, University of Chieti-Pescara, Viale Pindaro 42, 65129 Pescara, Italy; Research Associate, Istituto Nazionale di Geofisica e Vulcanologia, Italy. ORCID: https://orcid.org/0000-0001-5835-079X. Email: sara.amoroso@unich.it
[3] Res. Asst., Department of Civil and Environmental Engineering, Brigham Young University, 430 Engineering Building, Provo, Utah 84602, ORCID: https://orcid.org/0000-0003-0576-1207, email: paul.andersen@byu.edu
[4] Assoc. Prof., Dept. of Civil, Chemical, Environmental, and Materials Engineering, Univ. of Bologna, Viale del Risorgimento 2, 40136 Bologna, Italy, email: laura.tonni@unibo.it
[5] Pres. & Chief Engineer, Geopier Foundation Co., 130 Harbour Place Drive, Suite 280, Davidson, NC 28036, email: KWissmann@geopier.com

Keywords: Rammed Aggregate Piers, Silty Sand, Liquefaction, Liquefaction Mitigation, Liquefaction-Induced Settlement, Blast-Induced Liquefaction

INTRODUCTION

The amount of potential liquefaction-induced settlement in cohesionless soils is related to the initial state criteria of the soil. Looser soils have a higher void ratio, and a greater potential to contract under loading than more compact soils. During contraction the void ratio is reduced, causing settlement associated with volumetric strain. Many ground improvement techniques focus on densification of the soil, which reduces the void ratio and reduces the potential liquefaction-induced settlement. These techniques include vibro-compaction, rammed aggregate piers, stone columns, drilled displacement piles, driven displacement piles, deep dynamic compaction, blast-densification (Mitchell 1981, Han 2010). Vibratory compaction methods are common forms of densification for cohesionless soils, as both loose and medium dense sands will experience densification during vibration (Castro 1969). Extensive research has shown that vibrational ground improvement techniques are effective in densifying sands with less than about 15% fines (D'Appolonia 1954; Mitchell 1981; Baez 1995; Adalier and Elgamal 2004; Wissmann et al. 2015; Vautherin et al. 2017).

In contrast, vibratory compaction techniques become progressively less effective in silty sands as the fines content and plasticity increase (Saito, 1977, Mitchell, 1981) Leurhing et al. 2001). Increasing fines content strengthens the soil structure and decreases the permeability, preventing pore pressure dissipation, so that there is less densification. In these conditions, it may be necessary to increase the area replacement ratio (area of column/tributary area) to 20 to 25% and/or use prefabricated drains between columns to achieve significant improvement (Leurhing et al. 2001, Allen et al. 1995, Rollins et al. 2009) As fines content increases, other ground improvement techniques, such as vibratory replacement or soil mixing, are often preferred. Examples of such types of ground improvement are summarized by Han (2010). Vibratory replacement improves less compactible materials by the installation of load bearing columns of well-compacted, coarse-grained backfill material (Priebe 1995). These techniques mitigate against liquefaction by increasing soil density, increasing the mean stress, providing drainage for excess pore water pressures, and increasing the stiffness and shear resistance of the soil (Priebe 1998). Soil mixing creates a grid of soilcrete panels that provide increased lateral resistance and reduce the potential for liquefaction of sand within each grid (Namikawa et al. 2007).

Current CPT- and SPT-based liquefaction-induced settlement evaluation techniques typically account for increased density produced by various ground improvement methods and generally do not comprehensively consider other improvement mechanisms (Youd et al., 2001; Zhang et al., 2002). For RAPs, these mechanisms include composite response (Lawton and Fox 1994; Demir et al. 2017), increased lateral pressure (Harada et al., 2010), and increased shear stiffness (Green et al. 2008), which has been the subject of numerous recent studies for both RAPs and stone columns (Pestana and Goughenour 1999; Green et al. 2008; Olgen et al. 2008; Rayamajhi et al. 2010). Furthermore, there are only a limited number of published studies demonstrating RAP effectiveness in mitigating liquefaction in sandy silts and silty sands (Wissmann et al. 2015; Saftner et al. 2016; Smith and Wissmann 2018).

To better understand the mechanisms of RAP improvement for liquefaction mitigation, two full-scale blast tests were performed at a silty sand site in Bondeno, Italy (near Ferrara) where liquefaction was observed after the 2012 M_W 6.1 Emilia Romagna earthquake (Emergeo Working Group 2013), as preliminarily presented by Amoroso et al. (2019). Blast testing has been performed previously to evaluate lateral resistance of piles (Rollins et al. 2005), improvement from stone column treatment (Ashford et al. 2000; Weaver et al. 2004), improvement from colloidal silica grouting (Gallagher et al. 2007), improvement from driven displacement piles (Gianella and Stuedlein 2017), earthquake drain effectiveness (Rollins et al. 2004), and to compare a variety of ground improvement techniques in Christchurch, New Zealand (Wentz et al. 2015). In Bondeno, one blast test was performed around a profile treated with a group of 16 RAPs and referred to as the improved panel (IP), while another blast test was performed on an adjacent untreated natural panel (NP) to provide a control section for comparison. This paper compares the performance of the natural and improved panels in terms of excess pore pressure and settlement, then evaluates various models for computing settlement with measured profiles.

SITE LOCATION AND CHARACTERIZATION

The location of the Bondeno test site was selected based on surface evidence of liquefaction that was noted during the 2012 earthquake sequence in the region. Geotechnical in-situ tests were performed at a number of potential sites around Bondeno, until a suitable site was identified with a relatively uniform layer of liquefiable silty sand. A plan view drawing showing the locations of the natural and improved panels, defined by rings of blast holes, is provided in Fig. 1.

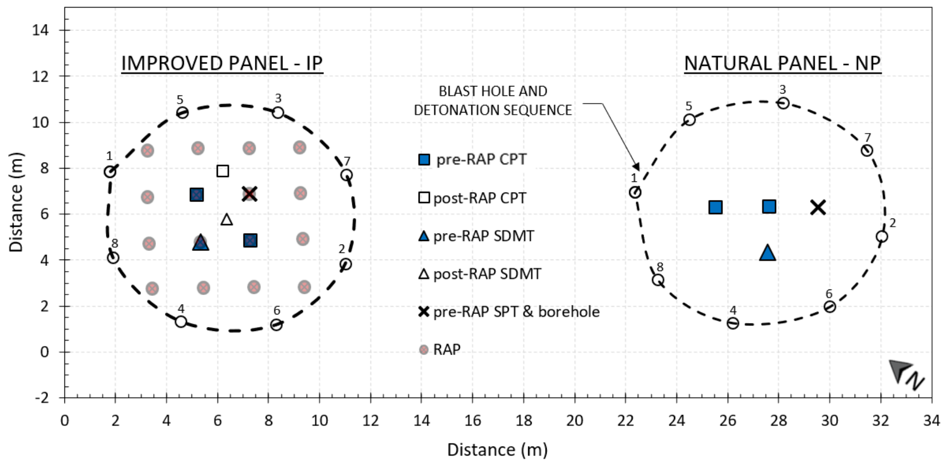

Fig. 1. Locations of in-situ tests and blast holes in the natural panel (NP) and improved panel (IP).

Results from the in-situ CPTu and DMT testing at the natural panel (NP) and improved panel (IP) before RAP installation (pre-treatment) are shown in Fig. 2. The CPTu sounding at both profiles was continued to 15 m depth. The DMT investigation in the IP was discontinued at 11.5 m depth due to technical difficulty advancing the dilatometer blade. As seen in Fig. 2, the profile consists of a surface layer composed of silty clay and clay (CL) to a depth of 3.5 m, underlain by silty sand (SM) to a depth of 12.6 m, which is in turn underlain by sands and silty sands (SP-SM). Geological investigations found that the silty sand layers from 3.5 to 12.6 m consist of Holocene alluvial deposits in a paleo channel of the Po River, while the deeper sand and silty sand layers are late Pleistocene glacial braided Po river deposits (Regione Emilia-Romagna 1998, Amoroso et al. 2020). The cohesive soil layer has an average plasticity Index of 20% and a I_c greater 2.6, therefore liquefaction and liquefaction-induced settlement would not be expected from 0 to 3.5 m below ground (Robertson and Wride 1998, Boulanger and Idriss 2016, Bray and Sancio 2006).

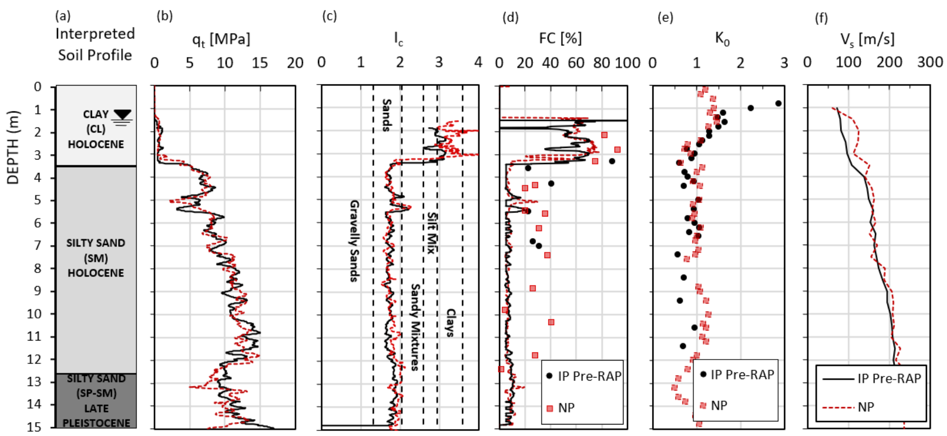

Fig. 2. (a) Interpreted soil profile and comparisons of CPTu and SDMT test results at the natural panel (NP) and the pre-RAP treatment improved panel (IP) with respect to (b) corrected cone tip resistance, q_t, (c) soil behavior type, I_c, (d) fines content, *FC* from Robertson and Wride (1998) correlation and disturbed samples, (e) earth pressure coefficient , K_0, and (f) shear wave velocity, V_s.

The corrected cone tip resistance (q_t) and the soil behavior type index (I_c) values from the CPTu are very similar for the NP and IP sites as are the fines contents estimated using a correlation proposed by Robertson and Wride (1998). However, measured fines contents in the sand layers are typically between 20 and 40%, and are considerably higher than interpreted from the correlation. This is consistent with results based on a 2600-point data set in Christchurch, New Zealand (Maurer et al. 2015), where significant scatter from predicted fines content was observed. In this study, the clean sand equivalent has been determined using the I_c value which is a function of both fines content and plasticity as suggested by Robertson and Wride (1998).

The profiles of the earth pressure coefficient (K_0), obtained from the DMT testing using the Marchetti (1980) formula, and of the shear wave velocity (V_s), measured according to Marchetti et al. (2008), also show reasonably good agreement between the two panels, particularly in the sand layers.

RAP GROUP LAYOUT AND RAP INSTALLATION

Over a three-day period, the 0.5 m diameter RAP columns were installed to a target depth of 9.5 meters in a 4x4 quadrangular grid covering a 6.5 m x 6.5 m area, with 2 m center-to-center spacing as shown in Fig. 3.

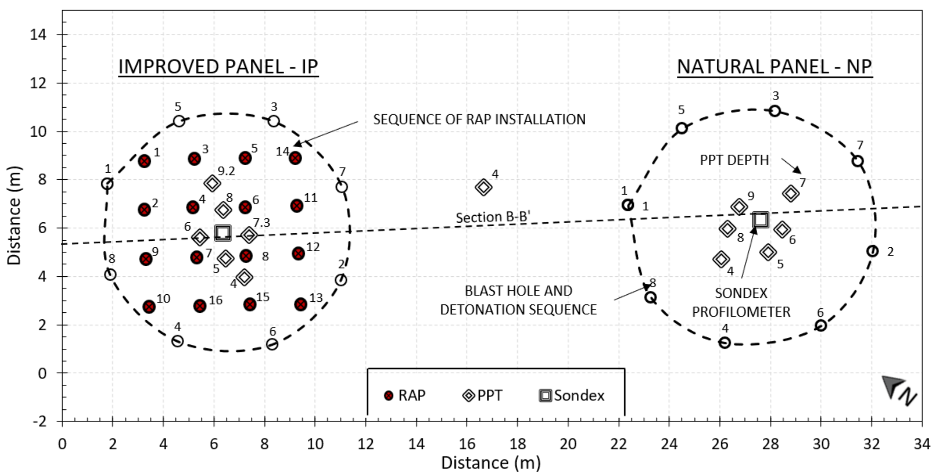

Fig. 3. Locations of blast holes, RAP columns, pore pressure transducers (PPTs), and profilometers for the natural and improved panels. Numbers by blast holes indicate detonation sequence, numbers by RAP columns indicate construction sequence, numbers by PPTs indicate depth.

The RAP elements were constructed by a local Geopier® affiliate, Releo, Inc, using displacement techniques with an excavator mounted mobile ram base machine fitted with a high frequency (30 to 40 Hz) vibratory hammer as illustrated in Fig. 4. The base machine drives a 250 to 300 mm outside diameter open-ended pipe mandrel fitted with a specially designed 350 to 400 mm diameter tamper foot into the ground. A sacrificial cap or internal compaction mechanism prevents soil from entering the tamper foot and mandrel during driving. After driving to the designed depth, the hollow mandrel serves as a conduit for aggregate placement. Placed inside, the aggregate flows to the bottom of the mandrel. The tamper foot and mandrel are then raised approximately 0.9 m and then driven back down 0.6 m, forming a 0.3 m-thick compacted lift. Compaction is achieved through static down force and dynamic vertical ramming from the hammer. The process densifies aggregate vertically and the beveled tamper foot forces aggregate laterally into the cavity sidewalls. This process typically required about 45 minutes of compaction for each 9.5 m long pier. The construction methods have been shown to increase the density of the pier aggregate to greater than 22 kN/m^3 (Lawton and Merry 2000) providing a friction angle greater than 45 degrees (White et al. 2002).

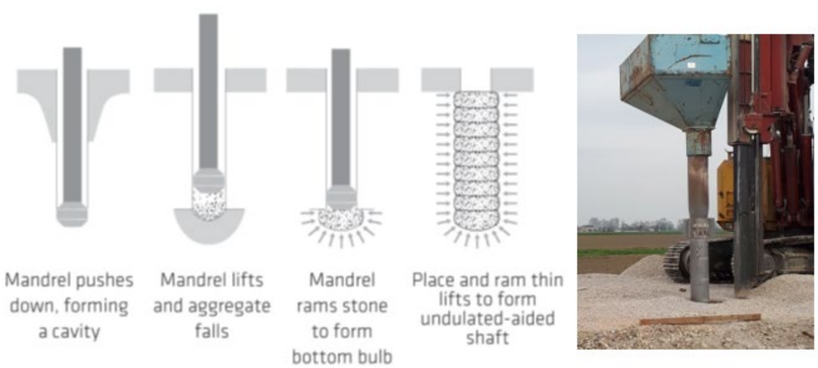

(a) (b)

Fig. 4. (a) Simplified representation of RAP construction process. (b) RAP installation at the Bondeno test site (after Amoroso et al., 2019).

Crushed aggregate was fed through the mandrel from a top mounted hopper and compacted in the displaced cavities to create a 0.5 m diameter, dense, stiff, aggregate pier element. The aggregate consisted of crushed limestone with an angular particle shape and a D_{50} size of 12.5 mm. The aggregate had a very uniform gradation with a C_u of 1.27 and a C_c of 0.94. The construction methodology has been described in more detail by Majchrzak et al. (2009) and Saftner et al. (2018).

The RAP installation process was intended to densify and increase the lateral earth pressure in the surrounding soil while constructing a dense aggregate column. The installation pattern produced an area replacement ratio (R_a), defined as the ratio of the pier area to the 2-m square tributary soil area surrounding the pier, equal to 5%. Based on experience, this area ratio was expected to increase the cone tip resistance by 1 to 4 MPa (20 to 30%) depending on the fines content and initial tip resistance. This was intended to increase the factor of safety against liquefaction (FS_L) above 1.25 for the design earthquake (M_W = 6.14, a_{max}= 0.22) or reduce settlement to less than about 2.5 cm. However, predicting improvement in silty sand is difficult and the experiment provides an opportunity to measure actual improvement based on a variety of in-situ tests.

Ten RAPs were evaluated using an index test known as a "Crowd Stabilization Test (CST)" at three depths in each pier during installation (Geopier Foundation Co., 2019). In these tests, a downward pressure of 140 MPa was applied to the pier by the installation machine and settlement was measured after 15 seconds. The average settlement for the first three piers was 123 mm, while the average for the remaining piers decreased to 18 mm. A settlement less than 25 to 50 mm is typical of a well compacted pier. Clearly, the first three piers were not as well compacted while the stroke pattern and mandrel lifting rate were being refined for the project. Two pilot piers would normally be used to make these adjustments for a commercial project. The order of installation of the pier numbers shown in Fig. 3. Fig. 6 provides a simplified cross-section after RAP installation along section B-B’ in Fig. 3.

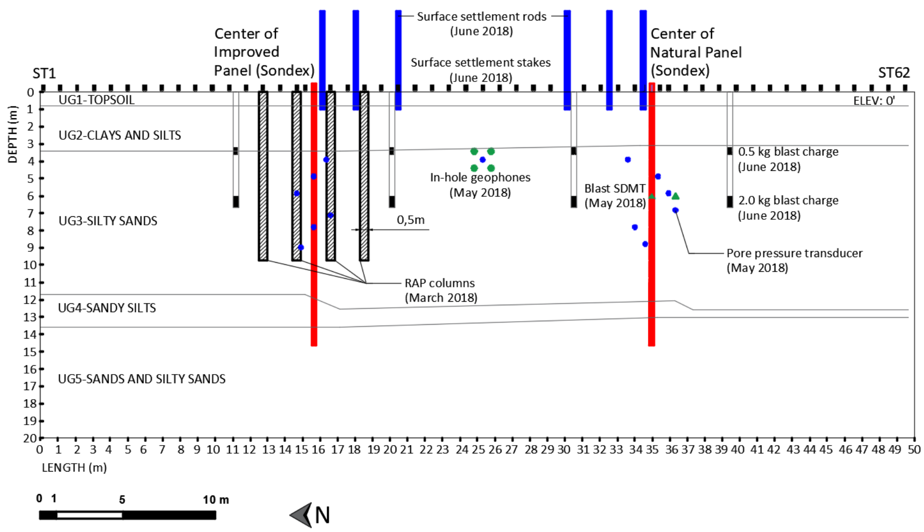

Fig. 5. Simplified soil profile showing the relative positions of the improved panel (IP) and the natural panel (NP), RAP column positioning, blast holes and other instrumentation at the site.

POST-RAP GROUND IMPROVEMENT EVALUATION

Additional geotechnical in-situ tests (CPTu and SDMT) were conducted at the center points between RAPs as shown in Fig. 3 after the installation of the RAP columns to quantify the improvement. Fig. 6 provides plots of the corrected cone tip resistance q_t, soil behavior type index I_c, relative density D_r, in situ earth pressure coefficient K_0 and FS_L. The pre-improvement plots are from one seismic dilatometer performed to 11.4 m depth, and the post-improvement characteristics are plotted from one seismic dilatometer performed between 0 and 4.8 m depth, and one medusa dilatometer performed between 4.6 and 11.2 m depth. The Medusa dilatometer is a new DMT device that combines the flat dilatometer with hydraulic automation and a measuring system for autonomously performing DMT tests (Marchetti et al. 2019). As anticipated, no improvement occurred from RAP installment in the clay layer between 0 and 3 m depth. Between the depths of 4 and 9 m the corrected cone tip resistance (q_t) and horizontal stress index (K_D) each experienced significant improvement one month after RAP installation, about 30% and 50%, respectively. The relative density computed using a correlation with CPT cone resistance (Jamiolkowski et al., 2003), also shows a moderate improvement (approximately 13%) within the layer of interest. The increase in K_D suggests a significant increase in lateral earth pressure due to RAP treatment. In sandy layers, K_0 can be estimated by coupling data from CPT and DMT data according to Baldi et al. (1986). Post-RAP K_0 values increased about 30% between 4 and 7 m depth and 100% between 7 and 9 m depth in comparison to the natural soil conditions.

The FS_L was computed using the well-established CPTu-based procedure proposed by Idriss and Boulanger (2008). The liquefaction susceptibility analyses were performed for a moment magnitude M_W = 6.14 (Meletti et al. 2008) and a peak ground acceleration, a_{max}= 0.22 (Stuchi et al. 2011). For this analysis, the water table was assumed to be at 0.5 m during the earthquake event. These values correspond to those used in ongoing seismic microzonation studies of the Bondeno municipality for a return period of 475 years. Prior to treatment, liquefaction would be predicted between 3.5 and 8 m with an average FS_L of 0.87. After treatment, the FS_L profile shows a significant increase with an average FS_L of 1.28 between 3.5 to 8 m. The FS_L increases most significantly in the zone between 5.5 and 8.0 m where the average I_c is 1.71, relative to the zone from 3.5 to 5.5 m where the average I_c is 1.82 and I_c exceeded 2.0 in two layers. Similar sensitivity of ground improvement to I_c variation has been observed for stone column treatment in silty sands (Rollins et al. 2012).

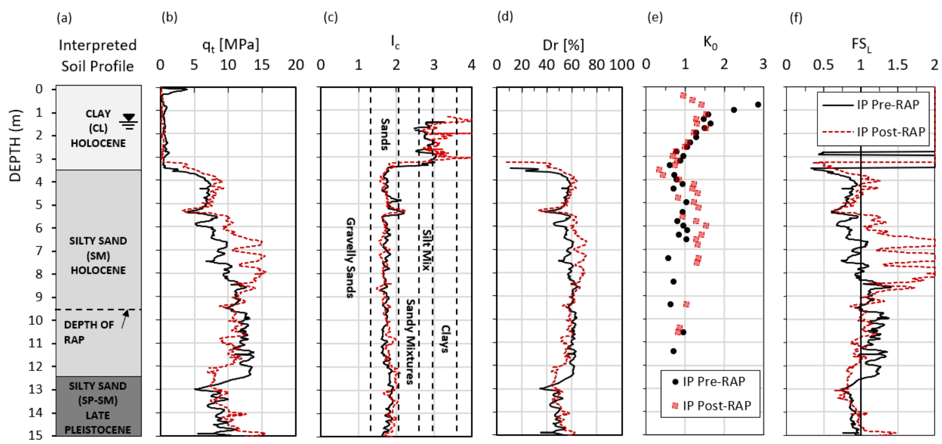

Fig. 6. Effects of RAP improvement within the (a) Interpreted soil profile, as measured by (b) q_t, (c) I_c, (d) D_r, (e) K_D, (f) FS_L.

BLASTING PROCESS AND INSTRUMENTATION LAYOUT

A total of 16 explosive charges were detonated during each blast test. The charges were placed around the periphery of two 10 m diameter circles as shown in Fig. 3. Eight blast holes were cased to a depth of 7 m at 45° intervals around the perimeter of the rings. Explosive charges (dynamite with a detonation velocity of 5900 m/s) were installed at two different levels within the liquefiable layer: 0.5 kg at 3.5 m and 2.0 kg at 6.5 m with gravel stemming between them to increase blast pressure in the horizontal direction. The explosive charges were detonated sequentially at one second intervals with detonation of the bottom charge followed by the upper charge in each blast hole. The sequence of blasting is indicated adjacent to the blast hole in Fig. 3 with blast holes alternating from opposite sides of the ring. The blasts of the two panels were conducted separately (i.e. blast 1 for the NP and blast 2 for the IP) to limit effects of superposition and simplify the comparison of the effects of the blast induced liquefaction on the IP and the NP, separately. At the center of each panel, a “Sondex” profilometer (resolution of 0.3 cm) was installed to a depth of 15 m to record the settlement vs. depth in the profile.

Pore pressure transducers (PPTs) were installed at depths of 4, 5, 6, 7, 8 and 9 m in each test panel at a distance of 1 to 2 m from the panel center (see Fig. 3) to measure the generation and subsequent dissipation of the excess pore pressures induced by the blast. The PPTs had a resolution to 0.7 kPa with a 3450 kPa maximum range and an overpressure limit of five times. Six survey poles were placed within the NP (P1, P2, P3) and the IP (P4, P5, P6) to monitor ground surface settlement with time after the blast. Conventional survey measurements were made using a Topcon DI-502 digital auto level, which measured ground surface settlements to 0.03 cm (0.001 ft) accuracy along a linear array of sixty-two survey stakes (ST) following each blast. Finally, Terrestrial Laser Scanning (TLS), and Structure from Motion (SfM) aerial photogrammetry was used to create point clouds and Digital Terrain Models (DTMs) that provided the overall pattern of ground surface settlement for each test blast.

Explosives were installed on the day of the blast for safety reasons. The first blast took place in the NP at 12:22:35 local time, followed by the second blast in the IP several hours later at 15:24:56 in order to study the effect of the blast-induced liquefaction on the NP and IP separately. The excess pore pressure ratio, r_u, returned to static levels approximately 6 and 5 minutes after the first and second blast sequences, respectively.

RESULTS FROM BLAST 1 AROUND NATURAL PANEL (NP) AND BLAST 2 AROUND IMPROVED PANEL (IP)

The pore pressure response and resulting settlement in the NP and the IP from the two identical blast events are compared in the subsequent sections.

Excess Pore Pressure Measurements

The excess pore pressure ratio (r_u), defined as the excess pore pressure (Δu) divided by the initial vertical effective stress (σ'_{vo}), was monitored during and after each blast sequence. Pore pressure transducer (PPT) measurements made at a sampling rate of 100 Hz, were smoothed with 100 point moving average to remove the majority of transient pulses and better represent the residual pore pressure. Plots of the residual excess pore pressure ratio versus time are provided in Fig. 7 (a) and (b) for the six transducers in the NP and IP, respectively. The inset plots in Fig. 7 (a) and (b) show each data point within the blast window and includes transient spikes during the blast sequence.

For each charge detonation a transient pressure spike developed followed by an increase in the residual excess pore pressure ratio. At both panels, excess pore pressures rapidly developed after a few seconds and remained at their peak for 15 to 20 seconds before dissipating. The r_u values dissipated from the bottom upwards and decreased to essentially static levels within about 6 minutes after blast detonation. In the improved panel, the blasting sequence generated somewhat lower peak r_u values and the dissipation rate was somewhat more rapid in comparison with the natural panel.

The peak residual r_u values for the IP and NP are plotted versus depth in Fig. 8. In the NP during blast 1 the peak measured r_u values are close to 1.0 from 3 to 9 m indicating liquefaction. In contrast, the peak r_u values in the IP during blast 2 are generally lower than 1.0 indicating that the RAP columns were effective in reducing the generation of excess pore pressures. The post-improvement D_r and K_0 profiles from Fig. 6 suggest that increased density and lateral earth pressures were in part responsible for the reduction in potential excess pore pressure generation. Significant r_u reductions from NP are seen at depths of 5, 7, 8 and 9 m. At these depths the peak residual r_u was kept below the 80% limit for incipient liquefaction suggested by Studer and Kok (1980). In both the NP and the IP larger r_u values were observed at depths of 4 and 6 m. These higher r_u values at 4 and 6 m are likely due to the co-planar placement of the blast charges at nearly corresponding depths. In the NP, the average peak r_u excluding the 4 and 6 m transducers was 95%, compared to 78% in the IP. Fig. 6 shows that for both the NP and the IP the rate of excess pore pressure dissipation recorded in the 4, 5, and 6 m PPTs was significantly slower than in the PPTs at 7, 8 and 9 m. During the blast sequence on the opposite side of the field, that is, the north side of the field for blast in the NP, and the south side of the field for blast in the IP, some level of r_u generation was produced. Fig. 8 shows that the r_u values were slightly higher in the NP than in the IP, though they were below the level for incipient liquefaction.

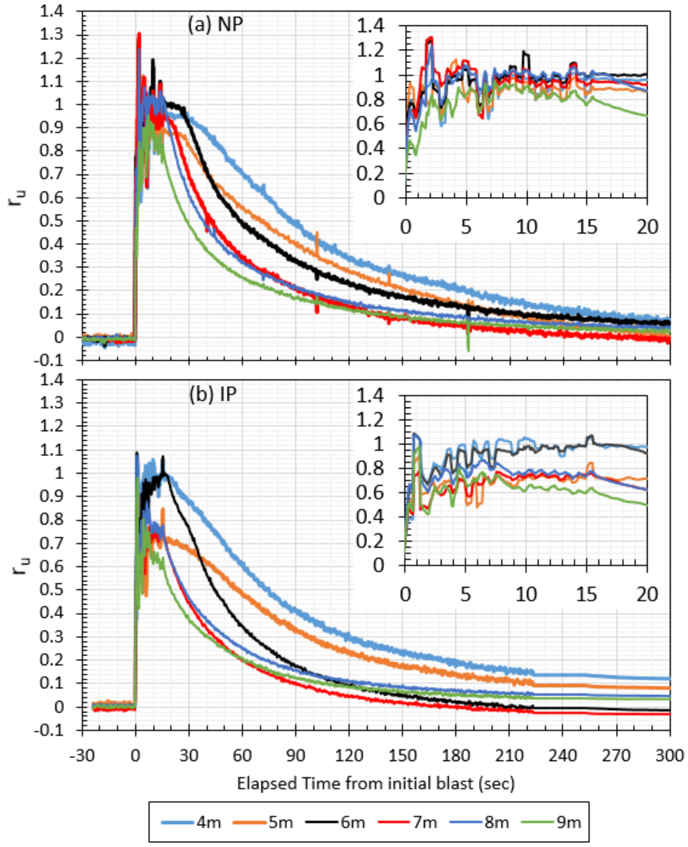

Fig. 7. Residual excess pore pressure ratio recorded during (a) blast 1 in the NP, and (b) blast 2 in the IP at 4, 5, 6, 7, 8 and 9 m depths. Average peak residual excess pore pressure ratio with depth immediately during blast (shown inset)

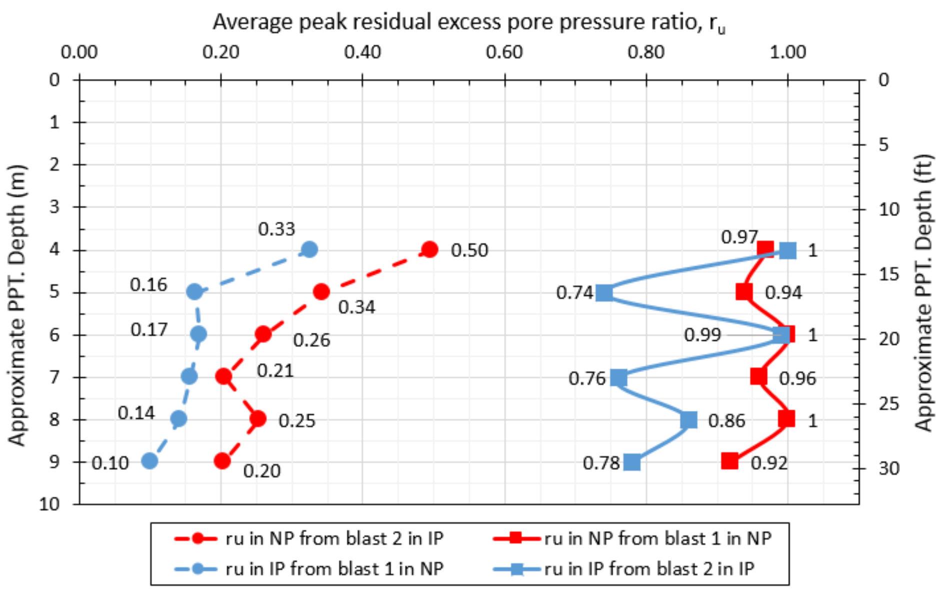

Fig. 8. Comparison of peak excess pore pressure ratio, r_u, measured during blast 1 in the natural panel (NP) and blast 2 in the improved panel (IP).

Sand Ejecta

Following blasting, several large sand boils developed within the blast ring in the natural panel as shown in the photograph in Fig. 9. These characteristic liquefaction features visually confirm the results of the pore pressure measurements. Mineralogical evaluation of the ejecta from the sand boil with sand from SPT testing indicates that the ejecta likely came from liquefaction in the depth interval between 3 and 9 m (Amoroso et al. 2019).

In contrast to the natural panel, no sand boils formed within the area treated with RAP columns, although smaller sand boils developed outside the treated zone. Considering that the development of ejecta was a major cause of building damage during liquefaction in the Christchurch earthquake sequence (van Ballegooy et al. 2014), this appears to be an important benefit of RAP treatment. Ejecta typically emerged at boreholes used to install instrumentation and blast holes; however, the same pathways existed in both the NP and the IP.

Fig. 9. Multiple sand boils and ejecta, evidence of liquefaction, observed during blast 1 near the center of the unimproved natural panel (NP).

Pore Pressure-Induced Settlements

Ground Surface Settlements. Ground surface settlements for blasts 1 and 2, based on elevation change of the survey stakes, are plotted in Fig. 10. Survey measurements were performed between 30 and 60 minutes after the blast when excess pore pressure had fully dissipated. Reconsolidation following blast-induced liquefaction produced a nearly symmetrical settlement pattern across the NP as shown in Fig. 10 for the first blast. Maximum settlement at the center of the blast ring was about 95 mm and settlement decreased to zero at a distance of about 12 m from the center of the blast ring. Settlements within the blast ring were between 70 and 95 mm after blast 1.

Elevation change was also measured using terrestrial laser scanning (TLS) and color contours of settlement after both blasts are provided in Fig. 11. The settlement contours indicate a circular dish-shaped settlement pattern in the natural panel similar to the autolevel, but the TLS settlements are somewhat lower. This is because sand ejecta accumulating at the ground surface decreases the settlement recorded by the TLS relative to that from the survey stakes. Additional details about the TLS based settlement are provided in Amoroso et al. (2020).

The settlement caused by the second blast is also shown in Fig. 10 along with the settlement induced by the first blast. The second blast produced both settlement within the IP and some additional settlement in the NP, that could have been due to strain softening during the first blast sequence. Both the TLS and autolevel surveys confirm that the settlement in the IP was between 20 and 50 mm, which is considerably less than that in the natural panel.

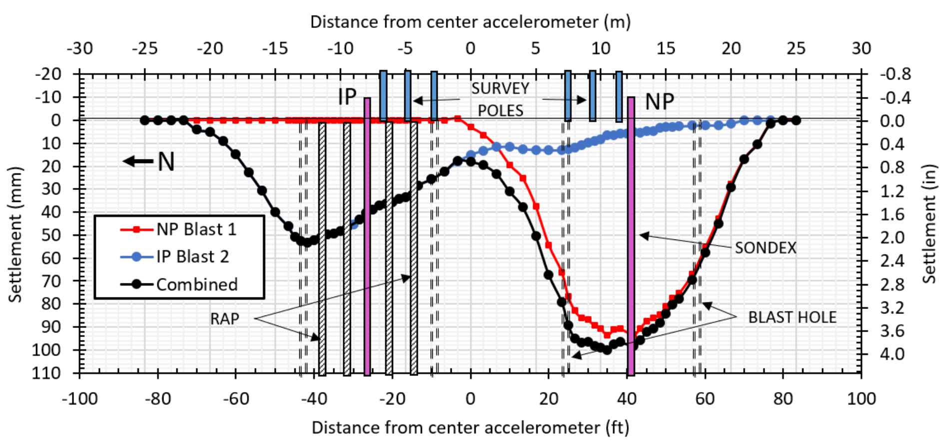

Fig. 10. A comparison of ground settlement measurements obtained 30 minutes after blast 1 in the NP, and blast 2 in the IP across the test field. The combined settlement from blast 1 and 2 is also plotted.

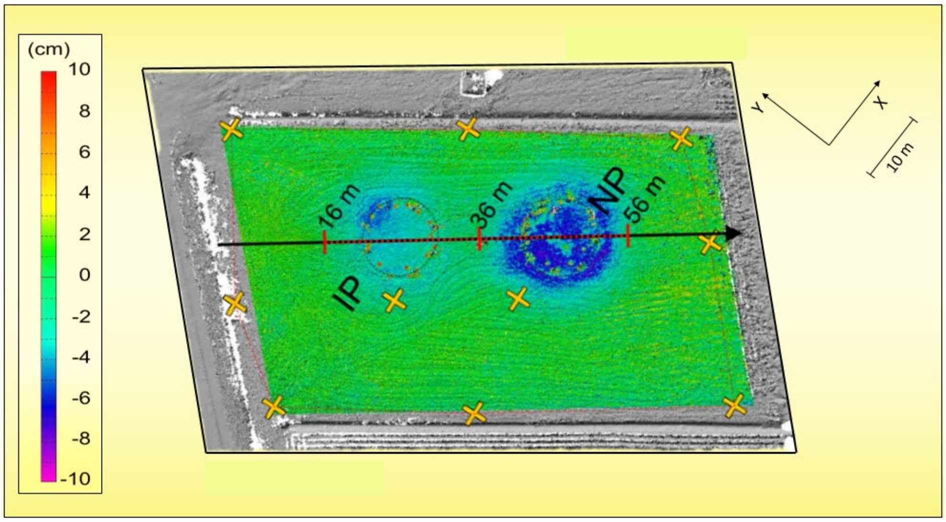

Fig. 11. Color contour map of cumulative settlement after the two blast tests from TLS surveys (After Amoroso et al. 2020).

The surface settlement from the second blast sequence did not exhibit a symmetric settlement profile, as was observed in the NP, but was higher on the north side (Fig. 10) and northeast corners of the panel (Fig. 11) relative to the rest of the treated area. One likely explanation for these higher settlements is the lower construction quality during the installation of the first three RAPs as described previously. The crowd stabilization test results demonstrate that the RAPs on the northeast side of the IP, that were the first to be constructed, settled more during crowd stabilization tests than the other RAPs in the grid. This lower RAP quality led to lower RAP column stiffness and less densification around these columns during treatment.

Settlement vs. Depth Measurements. Settlement vs. depth was also measured in both panels by the means of a Sondex profilometer, consisting of a corrugated pipe containing metal rings surrounding an access tube for a measurement probe. As the soil surrounding the corrugated pipe settled during pore pressure dissipation, the corrugated pipe is simultaneously compressed to match the soil settlement. The locations of the metal rings around the corrugated pipe are measured with a probe before and after blasting in order to compute the settlement. The settlement with depth in the NP as measured by the Sondex profilometer is provided in Fig. 12.

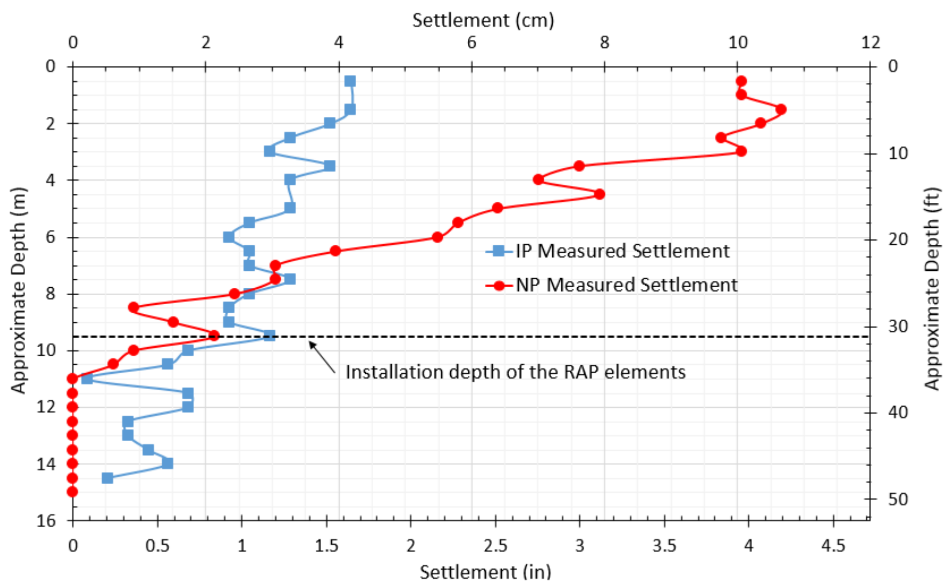

Fig. 12. Comparison of observed settlement with depth in the NP and the IP as measured by the "Sondex" profilometer after blasts 1 and 2, respectively.

The Sondex settlement provided data consistent with expectations based on soil stratigraphy and the measured ground surface settlement. The clay and organic soil within the top three meters did not compress, but settled along with the underlying sand. Liquefaction-induced settlement occurred within the layers of sandy-silt and silty-sand between 3 and 11 m depth. Below 11 m, the Sondex measurements in the NP area consistently showed that no settlement occurred indicating the pore pressure induced settlement was insignificant below 11 m. Average volumetric strain within the liquefied zone was approximately 1.6% from 3 to 8 m and approximately 0.8% from 8 to 11 m.

The settlement profile shown in Fig. 12 illustrates the significant reduction in settlement in the zone of RAP treatment (3-9.5 m) and a reduction of maximum surface settlement of approximately 6 cm. Of interest, the measurements indicate that less than 2 cm of compression occurred within the region of improvement in comparison to 8 cm of compression in the natural panel. In contrast to the profilometer in the NP, the settlement in the IP did not decrease to zero at a depth of 11 m although pore pressure induced settlement was likely insignificant below this depth as indicated by the natural panel settlement profile. This suggests that an additional mechanism may be responsible for the observed settlement of 1 cm below this depth. A few inconsistencies exist in the settlement with depth profiles provided in Fig. 12, such as the points where settlement appears to be less at shallow depth than at a deeper depth. These inconsistencies may be due to local slippage or irregular compression of the pipe.

Ground Surface Settlement vs. Time. Ground settlement due to liquefaction-induced reconsolidation was measured with time using autolevel readings on three survey poles embedded 0.5 m into the surface clay layer inside the blast ring. The autolevel tripod was positioned approximately 20 m NE and 35 m NE from the centers of the IP the NP, respectively, beyond the limit of ground settlement. The total settlements with time for the NP and IP are plotted in Figs. 13 (a) and (b), respectively. Settlement normalized by the maximum settlement for each pole is plotted in Figs. 13 (c) and (d), respectively. After normalization by the maximum settlement, the three settlement vs. time curves generally plot on top of each other. In the NP between 65-80% of the total settlement occurred within the first two minutes when the average r_u had decreased to 80%. Approximately 95% of the total settlement occurred within 13 minutes while the average r_u

values were nearly zero at 15 minutes. The average excess pore pressure ratio between 4 and 9 m depth dissipated to 60% of its initial value within 25 seconds of the final charge of the blast sequence.

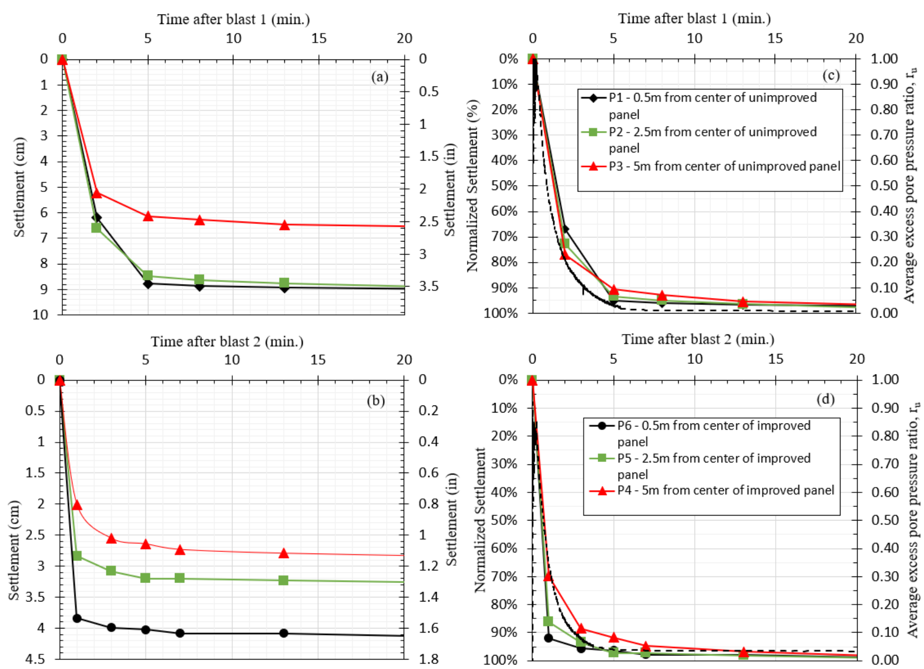

Fig. 13. Measured ground settlement with time for (a) NP for blast 1 and (b) IP for blast 2 along with settlement normalized by maximum settlement for (c) NP for blast 1 and (d) IP for blast 2.

In the improved panel, 95% of the settlement was completed within only 8 minutes, which is approximately 60% of the time required for 95% settlement in the NP. The increased rate of settlement is likely a result of horizontal drainage to the RAP columns in the improved panel. However, a lower modulus of compressibility in the silty sand would also have produced less water volume to be dissipated.

SETTLEMENT ANALYSIS

Computed settlement of the NP based on CPT resistance

The observed settlement profile in the natural panel indicates that liquefaction-induced settlement occurred between 3 and 11 m depth, as evidenced by Fig. 12. Little to no settlement occurred within the 3-m thick cohesive surface layer, that was non-liquefiable, and no settlement occurred below 11 m in the natural panel. Within the liquefied layers from 3 to 11 m, the CPT-based volumetric strain equations proposed by Zhang et al. (2002) were used to compute liquefaction-induced settlement relative to measured settlement in both the natural panel and the improved panel prior to the installation of the RAP columns. Zhang et al. (2002) use the cyclic liquefaction tests and reconsolidation settlement measurements from Ishihara and Yoshimine (1992) to develop volumetric strain equations. The Ishihara and Yoshimine curves are based only on relative density and FS_L. Zhang et al. (2002) developed a correlation to estimate relative density based on the normalized cone penetration resistance for clean sand $(q_{c1N})_{cs}$ obtained from I_c. One can then compute volumetric strain knowing $(q_{c1N})_{cs}$ and FS_L.

Although blasting clearly produced liquefaction based on pore pressure ratios and ejecta, the factor of safety against liquefaction in this case cannot be obtained using simple liquefaction triggering equations developed for earthquakes. However, the FS_L can be computed directly from the number of blast charges required to produce liquefaction in the field in comparison with the first eight large blast charges. Each blast charge typically produced one cycle of loading based on downhole ground motion recordings.

Seed and Idriss (1982) developed magnitude scaling factors (*MSF*) to adjust the cyclic resistance ratio (*CRR*) relative to a M_w7.5 earthquake producing 15 cycles of loading. When the *MSF* are plotted vs. the number of cycles as shown in Fig. 14, Seed and Idriss (1982) noted that the factor of safety against liquefaction (FS_L) for a soil that liquefied in 10 cycles relative to a total of 15 cycles could be given by the ratio of *MSF*s using the equation

$$FS_L = MSF_{15}/MSF_{10} = 1/1.13 = 0.88 \quad (1)$$

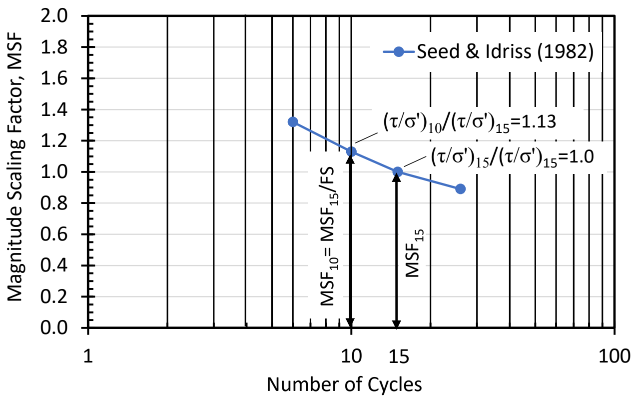

Fig. 14 Relationship between Magnitude Scaling Factor (MSF) vs. number of cycles to liquefaction and factor of safety against liquefaction (Seed and Idriss 1982).

Likewise, in our case, the equation can be generalized as

$$FS_L = MSF_8/MSF_{cycles\ to\ liquefaction} \quad (2)$$

because liquefaction generation was dominated by detonation of the first eight large charges. The blasting sequence was designed such that the larger 2.0 kg charges, triggered from 6.5 m depth, would generate the majority of the simulated earthquake energy, while the smaller 0.5 kg charges at 3.5 m depth would simply maintain excess pore pressures long enough to clearly observe behavior.

Using Eq. 2, an estimate for the FS_L was obtained at the depths of each PPT. The PPT data showed that r_u values reached about 1.0 by the fifth blast, or cycle of loading, at 4, 5, 6, and 8 m depth corresponding to a FS_L of 0.9. At depths of 7 and 9 m this did not occur until the eighth cycle of loading, corresponding to a FS_L of 1.0. Three *MSF* equations were used with Eq. 2 and produced comparable FS_L for the cycle ratios involved (Seed and Idriss 1982, Idriss and Boulanger 2008, and Kayen et al 2013).

Knowing FS_L, volumetric strain vs. depth could then be computed using the CPT-based equations developed by Zhang et al. (2002), for FS_L = 0.9 and 1.0, respectively:

$$\text{For } FS_L = 0.9, \qquad \varepsilon_v = 102(q_{c1N})_{cs}^{-0.82} \quad \text{for } 33 \leq (q_{c1N})_{cs} \leq 60 \tag{3}$$

$$\text{For } FS_L = 0.9, \qquad \varepsilon_v = 1430(q_{c1N})_{cs}^{-1.48} \quad \text{for } 60 \leq (q_{c1N})_{cs} \leq 200 \tag{4}$$

$$\text{For } FS_L = 1.0, \qquad \varepsilon_v = 64(q_{c1N})_{cs}^{-0.93} \quad \text{for } 33 \leq (q_{c1N})_{cs} \leq 60 \tag{5}$$

Settlement is simply the volumetric strain multiplied by the vertical layer thickness.

Settlement vs. depth plots were thus computed for the CPTu data at the NP area using the volumetric strain equations (Eq. 3 through 4) based on FS_L values of 1.0 and 0.9 for the appropriate layers. Fig. 15 (c) shows the computed settlement relative to the measured settlement along with the soil profile and normalized cone tip resistance ($q_{c1N,cs}$) in Fig. 15 (a) and (b), respectively. The computed settlement is in excellent agreement with the measured settlement vs. depth curve with an error of only 4% at the surface as shown in Fig. 15 (c).

Fig. 15 (c) also shows the computed settlement vs. depth curves for the pre-improvement IP using the same FS_L with depth. These estimates are within 3% of each other because there are only minor variations (1-2%) in the respective $q_{c1N,cs}$ profiles.

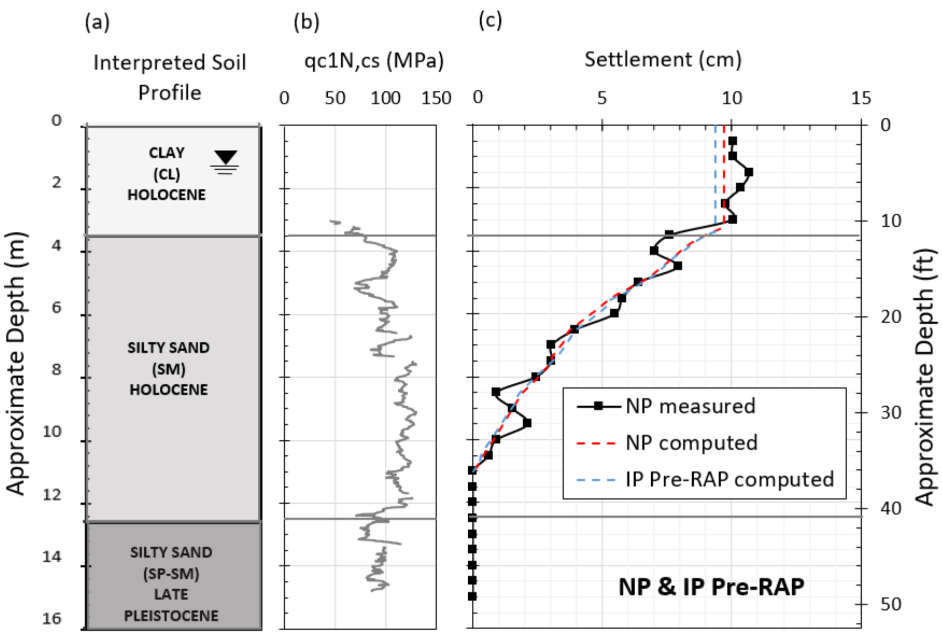

Fig. 5. (a) Simplified interpreted soil profile, (b) normalized pre-RAP CPT tip resistance with applied clean sand correction, (c) comparison of measured and computed settlement vs. depth curves in the NP and IP (pre-RAP) using the Zhang et al. (2002) volumetric strain equations based on CPT resistance.

This very good agreement with the measured settlement profile is somewhat surprising considering that post-earthquake field studies have found significant differences between and measured and computed ground settlement in Christchurch, New Zealand (Geylin and Maurer, 2019) and Urayasu, Japan (Katsumata and Tokimatsu, 2012). However, there are several factors that could explain this discrepancy. First, post-earthquake investigations often rely on SPT or CPT soundings made after the earthquake. After liquefaction, some layers will likely become denser while other layers will become looser (Whitman 1985, Seed 1987). In addition, after liquefaction, the soil microstructure produced by aging will be destroyed and may take many years to re-develop

(Andrus et al. 2009). These factors will lead to inaccurate settlement predictions from post-earthquake penetration testing. In contrast, the CPT soundings at the Bondeno site were all made before blast-induced liquefaction, avoiding all these problems.

Second, for typical field-case histories, the FS_L and the thickness of the liquefiable layer must be estimated using a triggering method based on CPT or SPT tests. Errors in these two factors compound the error in estimating settlement. In contrast, at this site, excess pore pressure and settlement were measured versus depth, so that the FS_L and thickness of the liquefied layer were well defined. Third, there is considerable uncertainty about the effect of fines content on liquefaction resistance, particularly with CPT-based triggering methods. This leads to variability in the predicted liquefaction thickness, the FS_L, and the resulting computed settlement. By contrast, fines content produced little uncertainty at this site because excess pore pressures were directly measured.

Finally, Cubrinovski et al. (2018) found that there was no difference in the average CPT penetration resistance in the critical liquefaction layers for sites that did and did not manifest liquefaction during the Christchurch earthquake sequence from 2010 to 2011. They attributed the difference in performance to the "system response" of the profile. Of course, the failure of the CPT to account for system response leads to errors in predicting the resulting settlement. It should be noted that the errors in settlement predictions reported by Geyin and Maurer (2019) were based on case history data from Christchurch. In contrast, at this site, there were no system response issues to complicate settlement calculations, which increases the potential for accurate assessment.

Computed Settlement of the IP based on Improved CPT Tip Resistance after RAP installation

The liquefaction-induced settlement following RAP installation was also computed in the IP using the Zhang et al. (2002) volumetric strain equations based on the post-installation $q_{c1N,cs}$ profile. Because the average measured peak residual r_u following the blast in the IP was approximately to 0.8, the FS_L was greater than 1.0. In this case, the FS_L was computed using a correlation with the measured r_u proposed by Tokimatsu and Yoshimi (1983) and confirmed by Ishihara (1985) as shown in Fig. 16. This approach was employed by the US Army Corps of Engineers for seismic evaluation of earth dams (Marcuson et al. 1990).

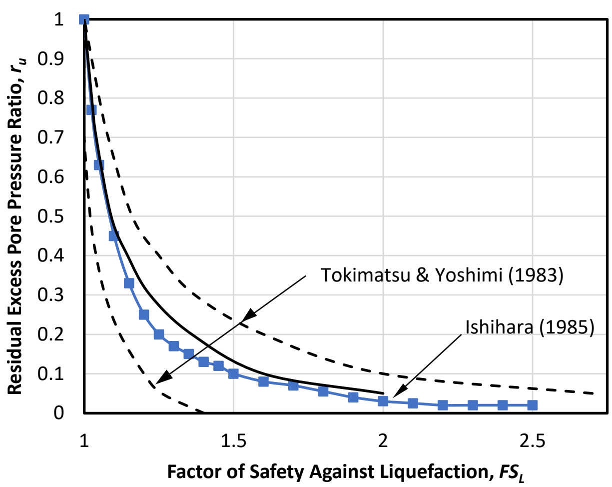

Fig. 16. Relationship between factor of safety against liquefaction (FS_L) and residual excess pore pressure ratio (r_u) (Tokimatsu and Yoshimi 1983, Ishihara 1985).

The FS_L was estimated for each meter of depth between 3 and 9 m according to the r_u measured by the nearest pore pressure transducer. To evaluate the sensitivity of FS_L on the settlement, upper-and lower-bound values of FS_L were also estimated using the Tokimatsu and Yoshimi (1983) correlation as shown in Fig. 17 (b). The FS_L varies between 1 and 1.06 for the test blast in the IP. The higher FS_L in the IP in comparison with the NP ($FS_L \approx$ 0.9-1.0) is thought by the authors to be attributable to both the increased relative density and increased lateral earth pressure of the improved soil. The liquefaction-induced volumetric strain for the varying FS_L at each depth was then interpolated between the curves provided by Zhang et al. (2002) for FS_L of 1.0 (Eq. 5) and 1.1 given by,

$$\text{For } FS_L = 1.1, \qquad \varepsilon_v = 11(q_{c1N})_{cs}^{-0.65} \quad \text{for } 33 \leq (q_{c1N})_{cs} \leq 200 \qquad (6)$$

The Zhang et al. (2002) method was also used to compute the volumetric strain for the zone beneath the limits of the RAP treatment (9.5 to 11 m) using the same approach for the untreated soil described previously.

The computed settlement versus depth curve is compared with the measured curve in Fig. 17 (c) and it is clear that the range in FS_L had very little effect on the computed settlement. The computed curve estimates a settlement of about 5 cm in the RAP treatment zone in comparison to the measured settlement of about 2 cm, which represents an overestimation of about 150%. This overestimation suggests that some other mechanism may be responsible for the reduction in settlement that occurred which will be explored in the next section.

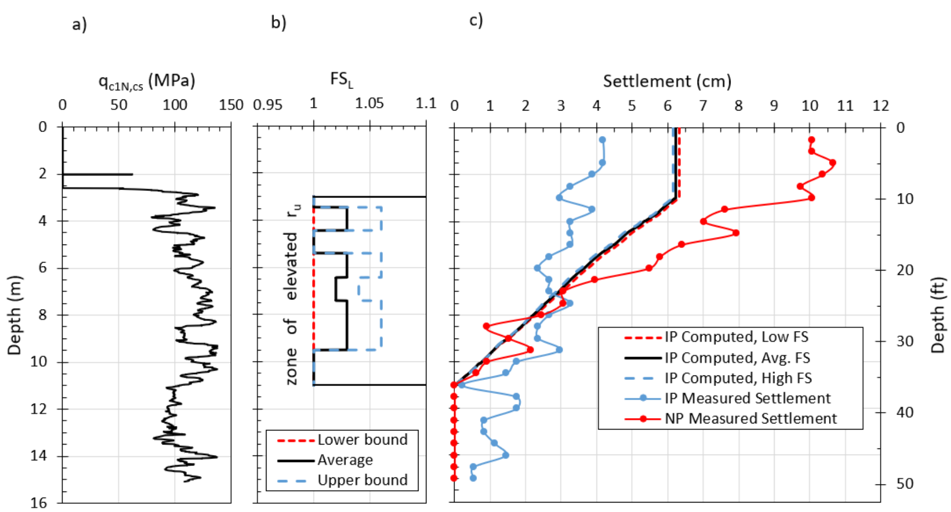

Fig. 6. (a) normalized CPT tip resistance with clean sand correction $(q_{c1N})_{cs}$ in the post-RAP IP, (b) upper-bound, average, and lower-bound values of FS_L with depth using the Tokimatsu and Yoshimi (1983) FS_L vs. r_u correlation, (c) observed settlement in the NP and the IP alongside the computed settlement in IP considering the effects of increased cone tip resistance using volumetric strain equations from Zhang et al. (2002).

Computed Settlement of the IP Based on Improved CPT Tip Resistance Combined with RAP Axial Stiffness

The predicted settlement of the IP using the Zhang (2002) volumetric strain equations in the previous section neglects the axial stiffness of the RAPs during liquefaction. Axial stiffness was recognized by Martin et al. (2004) to be an important part of settlement reduction for a site treated with jet grouted columns during the M_w 7.6 Kocaeli earthquake in Turkey. Moreover, Adalier et al. (2006) reported that stone columns in a silt matrix reduced foundation settlement by 50% owing to the increased average soil stiffness despite liquefaction in the silt matrix. Finally, Lawton and Fox (1994) recommend a composite modulus approach to consider the axial stiffness of the RAP in computing soil settlement after RAP treatment.

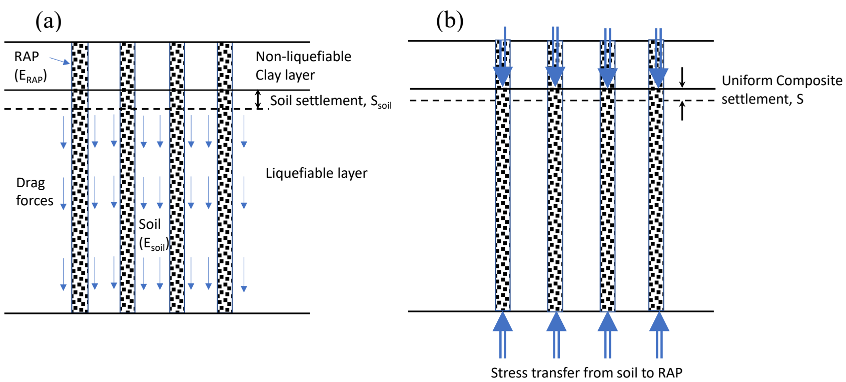

Fig. 18 Schematic drawing illustrating (a) settlement of soil, S_{soil}, with constrained modulus (M_{soil}) transferring load to stiffer non-liquefied RAPs with higher modulus (M_{RAP}) to produce (b) reduced uniform composite settlement, S, with increased load in the RAPs.

Fig. 18 shows a schematic drawing of the response of the treated ground as a result of post-blast liquefaction settlement. Fig. 8 shows that the blasting increased the pore water pressure in the IP to r_u values ranging between 0.74 and 0.97, with a consequent reduction in vertical effective stress. The post-blast dissipation of these pore water pressures reinstates the vertical effective stress resulting in settlement in the soil that may be predicted using the Zhang (2002) equations as in shown Fig. 17. Post-liquefaction settlements result in downward movement of the soil relative to the dense non-liquefiable RAPs resulting in stress transfer from the soil to the RAPs, which decreases the value of reinstated vertical effective stress in the soil and increases the effective vertical stress in the RAPs. The amount of stress transfer depends on the relative stiffness of the materials and the boundary conditions at the top and bottom of the system. For conditions in which the top and bottom boundary conditions are rigid, the settlement (S) is uniform and may be estimated using a simple expression:

$$S = \frac{qIH}{M_{composite}} \tag{7}$$

where q is the applied change in pressure, I is an influence factor (unity), H is the layer thickness, and $M_{composite}$ is the composite constrained modulus value. Values for q may be estimated as the reinstated vertical effective stress value computed as the product of the initial vertical effective stress and the layer r_u value. The composite constrained modulus value may be estimated from the average constrained modulus value for the post-blast response of the soil (M_{soil}), the post-blast constrained modulus of the RAP (M_{RAP}), and the area replacement ratio of the RAP (R_a) with the equation

$$M_{composite} = M_{soil}\,(1 - R_a) + M_{RAP}\,R_a \tag{8}$$

The post-blast constrained modulus value for the soil may be back-calculated using the equation

$$M_{soil} = \frac{qIH}{S_{soil}} \tag{9}$$

where q is the reinstated vertical effective stress value in the soil layer computed as the product of the initial vertical effective stress and the average layer r_u value, I is unity, and S_{soil} is the settlement of the soil between the RAPs after treatment computed using the Zhang et al. (2002) approach, equal to 5 cm as described in the previous section and shown in Fig. 17(c).

The post-blast constrained modulus (M_{RAP}) for the RAPs may be computed using the standard equation relative to the elastic modulus multiplied by a reduction factor for reduced confining pressure,

(10)

$$M_{RAP} = \frac{E_{RAP}(1-\nu)(R_\sigma)}{(1+\nu)(1-2\nu)}$$

where poisson's ratio (ν) is 0.3 and the elastic modulus value for the RAP (E_{RAP}) is taken as 192 MPa (4000 ksf) based on the average elastic modulus from a database of full-scale field load tests on RAP (Wissmann et al. 2001). For a large project in practice, a load test could be performed on a pier to directly determine the elastic modulus. When excess pore pressures develop in the soil surrounding a RAP, the effective confining pressure decreases, reducing the modulus as a function of the square root of the decreased pressure (Duncan and Chang 1970). The reduction in modulus can then be estimated using a reduction factor (R_σ) given by the equation

$$R_\sigma = \left[1 - \frac{(r_u)_{avg}}{2}\right]^{0.5} \tag{11}$$

where $(r_u)_{avg}$ is the average excess pore pressure ratio in the treated zone after blasting (or an earthquake) and $(r_u)_{avg}/2$ is the average excess pressure during reconsolidation to static water pressure. Using Eq. 10 and 11, the post-blast M_{RAP} for $(r_u)_{avg}$ of 0.86 in this case would be

195 MPa. Based on Eq. 8, with an area replacement ratio of only 5%, the piers account for 53% of the modulus and increase the $M_{composite}$ by a factor of 2.1 relative to M_{soil}.

Applying Eq. 7, yields a settlement of 1.86 cm in the treated zone from 3 to 9.5 m relative to the measured value of about 2.0 cm. Applying Eq. 7 incrementally, produces the computed settlement vs. depth profile in Fig. 19 that is in good agreement with the measured curve. Variations of ± 25% in the value of M_{RAP} lead to variations in the computed settlement of about ± 15% as shown in Fig. 19. The applicability of the composite settlement approach is also corroborated by the noted uniformity of the surficial settlements postulated in Fig. 18(b) and observed both visually and in TLS plot shown in Fig. 11.

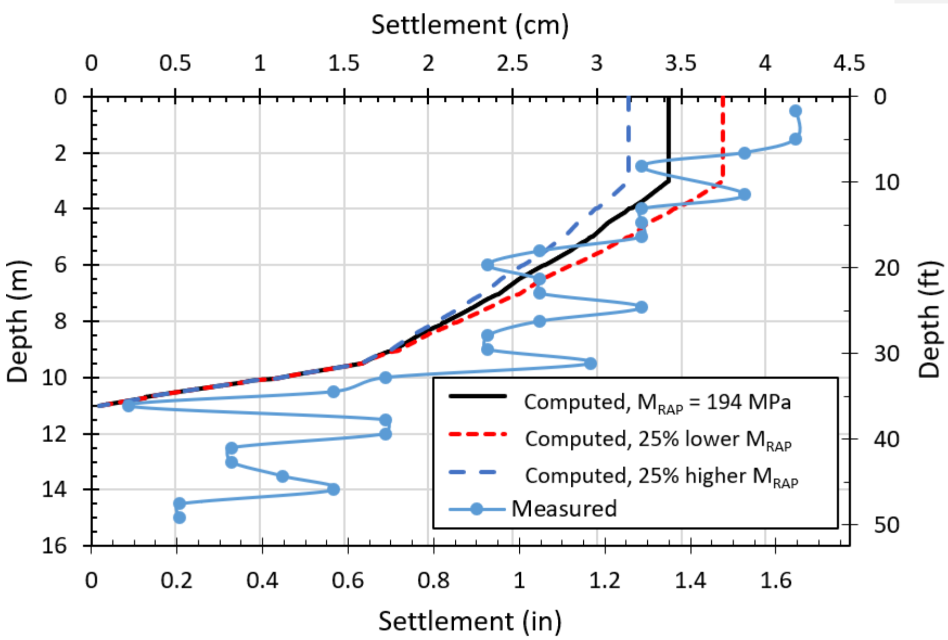

Fig. 19. Comparison of measured settlement vs. depth with settlement curves computed using a composite modulus approach with best-estimate M_{RAP} and ± 25% higher and lower MRAP values in the IP.

Commentato [KR1]: Change legend to "Computed, M_{RAP}=194 MPa", "Computed 25% higher M_{RAP}", and "Computed 25% lower M_{RAP}" and "Measured"

It seems reasonable to expect that other methods for installing dense granular columns (DGCs) may also be able to reduce liquefaction induced settlement by similar mechanisms to those presented for the RAP group in this study. However, similar field testing would be desirable to ensure this performance and field test data defining DGC stiffness would be necessary.

SUMMARY AND CONCLUSIONS

Full-scale blast-induced liquefaction tests were carried out in Bondeno, Italy to evaluate the effectiveness of Rammed Aggregate Pier (RAP) treatment in mitigating liquefaction hazards in

Holocene silty sands (fines content ≈ 15-45%). Blast tests were performed on natural and improved panels at a test site where silty sands liquefied and produced numerous sand boils during the 2012 M_w 6.1 Emilia Romagna earthquake. The RAPs consisted of 0.5 m diameter dense gravel columns installed to a target depth of 9.5 meters in a 4x4 arrangement at 2 m center-to-center spacing with a replacement ratio of 5%. The consistent nature of the soil profile between the natural and improved panels provided an excellent window for observing the mitigating effects of RAP improvement related to liquefaction. Pore pressure transducers and settlement monitoring provided detailed information about performance of the two panels.

Based on the field testing and subsequent data analysis, the following conclusions can be drawn:

1. Blasting produced liquefaction and induced settlement of 8.5 cm in the natural panel (NP) from 3 to 9.5 m. Several large sand boils developed following blasting. The computed settlement versus depth curve using the CPT-based volumetric strain equations proposed by Zhang et al. (2002) produced very good agreement with the measured curve.

2. RAP installation densified the silty sand, increasing q_c by about 30%. Post-RAP K_0 values increased about 30% between 4 and 7 m depth and 100% between 7 and 9 m depth in comparison to the natural soil conditions.

3. Installation of the RAP group decreased settlement after blasting to about 2 cm within the treated zone from 3 to 9.5 m, relative to 8.5 cm in the untreated area (76% improvement), despite the fact that r_u values of 74 to 100% still developed within the soil between the RAPs. No sand boils erupted within the treated area in the improved panel (IP).

4. The reduction in excess pore pressure-induced settlement in the IP could not be reasonably explained by the densification measured by the post-treatment CPT soundings. The Zhang et al.

(2002) CPT-based volumetric strain equations overestimated the measured settlement by 150% when considering densification effects alone.

5. The measured settlement versus depth profile within the RAP treatment zone was reasonably well computed assuming that the RAPs stiffen the surrounding sand and resist liquefaction-induced compression as a composite during pore pressure dissipation.

DATA AVAILABILITY STATEMENT

Some or all data, models, or code that support the findings of this study are available from the corresponding author upon reasonable request. These data include in-situ test results, excess pore pressure response, settlement vs. depth curves, and settlement vs. time curves.

ACKNOWLEDGEMENTS

Financial support for this study was primarily provided by Geopier® Foundation Company along with local affiliate Releo s.r.l. (Ferrara, Italy) who provided the installation of the Rammed Aggregate Piers free of charge. In addition, funding for Mr. Anderson was provided by an REU supplement to grant CMMI-1663288 from the National Science Foundation. This funding is gratefully acknowledged. However, the opinions, conclusions and recommendations in this paper do not necessarily represent those of the sponsors. From the Italian side, additional funding was provided by INGV-FIRB Abruzzo project ("Indagini ad alta risoluzione per la stimadella pericolosità e del rischio sismico nelle aree colpite dal terremoto del 6 aprile 2009", http://progettoabruzzo.rm.ingv.it/it), by the INGV-Abruzzo Region project ("Indagini di geologia,sismologia e geodesia per la mitigazione del rischio sismico", L.R. n. 37/2016), and by the CIRI Edilizia e Costruzioni, University of Bologna, Italy (TIRISICO PROJECT "Tecnologie

Innovative per la riduzione del rischio sismico delle Costruzioni", Project no. PG/2015/ 737636, POR-FESR 2014-2020). We also express our appreciation to the Bondeno Municipality and to the Emilia-Romagna Region who provided all the necessary support to realize the research in collaboration with the other local authorities (Ferrara Prefecture, Ferrara Province, Local Civil Protection, Police).

REFERENCES

Adalier, K., and Elgamal, A. 2004. "Mitigation of liquefaction and associated ground deformations by stone columns." *J. Engineering Geology*, 72(3-4), 275-291.

Adalier, K. Elgamal, A., Meneses, J., Baez, J.I. 2003. "Stone columns as liquefaction countermeasure in non-plastic silty soils." Soil Dynamics and Earthquake Engineering, 23(7), 571-584

Allen, M.G., Jones, R., Gularte, F.B. 1995. "Bottom-feed stone columns, wet-replacement construction method Mormon Island Auxillary Dam modifications." Soil Improvement for Earthquake Hazard Mitigation, GSP 49, ASCE, p. 82-93.

Amoroso, S., Rollins, K.M., Andersen, P., Gottardi, G., Tonni, L., García Martínez, M.F., Wissmann, K., Minarelli, L., Comina, C., Fontana, D., De Martini, P.M., Monaco, P., Pesci, A., Sapia, V., Vassallo, M., Anzidei, M., Carpena, A., Cinti, F., Civico, R., Coco, I., Conforti, D., Doumaz, F., Giannattasio, F., Di Giulio, G., Foti, S., Loddo, F., Lugli, S., Manuel, M.R., Marchetti, D., Mariotti, M., Materni, V., Metcalfe, B., Milana, G., Pantosti, D., Pesce, A., Salocchi, A.C., Smedile, A., Stefani, M., Tarabusi, G., and Teza, G. 2020. "Blast-induced liquefaction in silty sands for full-scale testing of ground improvement methods: insights from a multidisciplinary study." *Engineering Geology*. 265: 105437. https://doi.org/10.1016/j.enggeo.2019.105437

Amoroso, S., Rollins, K.M., Andersen, P., Gottardi, G., Tonni, L., García Martínez, M.F., Wissmann, K., and Minarelli, L. 2019. "Full-scale testing of liquefaction mitigation using rammed aggregate piers in silty sands." In *Proc., 7th International Conference on Eartquake Geotechnical Engineering – 7 ICEGE*. London, United Kingdom: Taylor and Francis Group. https://doi.org/10.1201/9780429031274

Amoroso, S., Rollins, K.M., Monaco, P., Holtrigter, M., and Thorp A. 2018. "Monitoring Ground Improvement using the Seismic Dilatometer in Christchurch, New Zealand." *Geotechnical Testing Journal*. 41(5): 946-966. https://doi.org/10.1520/GTJ20170376

Andrus, R.D., Hayati, H., Mohanan, N.P. (2009). "Correcting liquefaction resistance for aged sands using measured to estimated velocity ratio." J. Geotechnical and Geoenv. Engrg. ASCE, 135(6), p. 735-744, **DOI:** 10.1061/_ASCE_GT.1943-5606.0000025

Ashford, S.A., Rollins, K.M., Bradford, S.C., Weaver, T.J., Baez, J.I. 2000. "Liquefaction Mitigation Using Stone Columns Around Deep Foundations: Full Scale Test Results." *Transportation Research Record* 1736: 110-118. Transportation Research Board. https://doi.org/10.3141/1736-14

Baez, J.I. 1995. "A Design Model for the Reduction of Soil Liquefaction by VibroStone Columns." Ph.D Thesis, University of Southern California.

Baldi, G., Bellotti, R., Ghionna, V., Jamiolkowski, M., Marchetti, S. and Pasqualini, E. 1986. "Flat Dilatometer Tests in Calibration Chambers." In Proc., Specialty Conf. on Use of In Situ Tests in Geotechnical Engineering: Geotechnical Special Publication No. 6, 431–446. Reston, VA: ASCE.

Castro, G. 1969. "Liquefaction of sands." *PhD Dissertation,* Harvard University; reprinted as *Harvard Soil Mechanics Series* 81: 112 pp.

Bray, J.D. and Sancio, R.B. 2006. "Assessment of the liquefaction susceptibility of fine-grained soils" J. Geotechnical and Geoenviron. Engrg., ASCE,132(9): 1165-1177.

Boulanger, R.W. and Idriss, I.M. 2006. "Liquefaction susceptibility criteria for silts and clays." J. of Geotechnical and Geoenviron. Engrg., ASCE,142(2), 1413-1426.

Cubrinovski, M., Rhodes, A., Ntritsos, N., and Van Ballegooy, S. 2018. "System response of liquefiable deposits." *J. Soil Dynamics and Earthquake Engineering*, Elsevier, 124 p. 212-229, https://doi.org/10.1016/j.soildyn.2018.05.013

D'Appolonia, E. 1954. "Loose Sands - Their Compaction by Vibroflotation." in *Symposium on Dynamic Testing of Soils*, edited by Committee D-19 on Soils (West Conshohocken, PA: ASTM International, 1954), 138-162.

Demir, S., Özener, P., Kirkit, M., and Özener, P. 2017. "Experimental and numerical investigations of behavior of Rammed Aggregate Piers," *Geotechnical Testing Journal* 40(3), 411-425.

Duncan, J.M. and Chang, C-Y. 1970. "Nonlinear analysis of stress and strain in soils." J. Geotechnical and Geoenviron. Engrg., ASCE, 96(5), 16929-1653.

Emergeo Working Group. 2013. Liquefaction phenomena associated with the Emilia earthquake sequence of May-June 2012 (Northern Italy). *Natural Hazards and Earth System Sciences* 13 (4): 935-947.

Gallagher, P., Conlee, C.T., Rollins, K.M. 2007. "Full-Scale Field Testing of Colloidal Silica Grouting for Mitigation of Liquefaction Risk." *J. of Geotechnical and Geoenvironmental Engrg*., ASCE, 133(2), 186-196. https://doi.org/10.1061/(ASCE)1090-0241(2007)133:2(186).

Geopier Foundation Company 2019. "Rammed aggregate pier® construction and quality control procedures for the Impact® system, version 6", Davidson, North Carolina, 37 p.

Geyin, M. and Maurer, B.W. 2019. "An analysis of liquefaction-induced free-field ground settlement using 1,000+ case-histories: observations vs. s tate-of-practice predictions." *Geocongress 2019: Earthquake Engineering and Soil,* Geotechnical Special Publication 308: 489-498, ASCE.

Gianella, T.N. and Stuedlein, A.W. 2017. "Performance of driven displacement pile-improved ground in controlled blasting field tests." J. Geotechnical and Geoenviron. Engrg. ASCE, 143(9). DOI: 10.1061/(ASCE)GT.1943-5606.0001731.

Green, R.A. Olgun, C.G., Wissmann, K.J. 2008. “Shear Stress Redistribution as a Mechanism to Mitigate the Risk of Liquefaction.” Geotechnical Earthquake Engineering and Soil Dynamics IV, ASCE, Geotechnical Special Publication 181.

Goughnour, R.R. and Pestana, J.M. (1998). "Mechanical Behavior of Stone Columns Under Seismic Loading." Proc. 2nd International Conference on Ground Improvement Techniques, Singapore

Jamiolkowski M., Lo Presti D.C.F. and Manassero M. 2003. Evaluation of Relative Density and Shear Strength of Sands from Cone Penetration Test and Flat Dilatometer Test. *Soil Behaviour and Soft Ground Construction*; GSP 119: 201-238.Majchrzak, M., Farrell, T. & Metcalfe, B. 2009.

Katsumata, K. and Tokimatsu, K. 2012. “Relationship between seismic characteristics and soil liquefaction of Urayasu city induced by the 2011 Great East Japan Earthquake.” Procs. 9th Intl. Conf. on Urban Earthquake Engineering, Tokyo Institute of Technology, p. 601-606.

Lawton, E. C. and Fox, N.S. 1994. “Settlement of Structures Supported on Marginal or Inadequate Soils Stiffened with Short Aggregate Piers,” Proceedings of Settlement ’94, College Station, Texas, ASCE Geotechnical Publication No. 40, Vertical and Horizontal Deformations of Foundations and Embankments, ASCE, vol. 2, 962–974.

Lawton, E.C., and Merry, S.M. (2000). "Performance of geopier reinforced soil foundations during simulated seismic tests on I-15 bridge bents," Transportation Research Record No. 1736: Soil Mechanics 2000, Transportation Research Board, Washington, D.C. pp. 3-11.

Luehring, R., Snortland, N., Stevens, M. and Mejia, L. (2001). Liquefaction Mitigation of a Silty Dam Foundation Using Vibro-Stone Columns and Drainage Wicks: A Case History at Salmon Lake Dam,” Bureau of Reclamation Water Operation and Maintenance Bulletin, No. 198, 1-15.

Majchrzak, M., Farrell, T., Metcalfe, B. 2009. “Innovative Soil Reinforcement Method to Control Static and Seismic Settlements.” *Proceedings from International Foundation Congress and Equipment Expo*, Orlando, March 15-19, 2009.

Marchetti, S., Monaco, P., Totani, G., and Calabrese, M. 2001. “The Flat Dilatometer Test (DMT) in Soil Investigations – A Report by the ISSMGE Committee TC16.” Proc., 2nd Int. Conf. on the Flat Dilatometer, R. A. Failmezger and J. B. Anderson, eds., In-Situ Soil Testing, Lancaster, VA,7–48.

Marchetti, S. 1980. “In situ tests by flat dilatometer.” J. Geotech. Eng. Div. 106 (3): 299–321.

Marchetti, D., Monaco, P., Amoroso, S., Minarelli, L., 2019. In situ tests by Medusa DMT. In: Proceedings of the XVII European Conference on Soil Mechanics and Geotechnical Engineering ECSMGE-2019, Reykiavik, Iceland, https://doi.org/10.32075/17ECSMGE-2019-0657.

Marcuson, W.F. III, Hynes, M.E., and Franklin, A.G. 1990. “Evaluation and use of residual strength in seismic safety analysis of embankments.” Earthquake Spectra, EERI, 6(3), 529-572.

Martin, J.R., Olgun, C.G., Mitchell, J.K. and Durgunoglu, H.T. 2004. “High-modulus columns for liquefaction mitigation.” J. Geotechnical and Geoenviron. Engrg., ASCE, 130(6), 561-571.

Maurer, B.W., R.A. Green, S. van Ballegooy, L. Wotherspoon, 2019. “Development of region-specific soil behavior type index correlations for evaluating liquefaction hazard in Christchurch, New Zealand.” Soil Dynamics and Earthquake Engrg. 117, 96-105.

Meletti C., Galadini F., Valensise G., Stucchi M., Basili R., Barba S., Vannucci G., Boschi E.; 2008: A seismic source zone model for the seismic hazard assessment of the Italian territory. Tectonophysics, 450, 85– 108.

Mitchell, J. 1981. “Soil improvement – state-of-the-art report.” *Proceedings of the 10th International Conference on Soil Mechanics and Foundation Engineering*, Stockholm, 4, 509-565.

Namikawa, T., Koseki, J., and Suzuki, Y. 2017. “Finite element analysis of lattice-shaped round improvement by cement-mixing for liquefaction mitigation.” Soils and Foundations, Japanese Geotechnical Society, 47(1), p. 559-576.

Priebe, H.J. 1995. “The design of vibro replacement.” *Ground Engineering* 28(10): 31-46. https://doi.org/10.1016/0148-9062(96)80092-1

Priebe, H.J. 1998. “Vibro replacement to prevent earthquake induced liquefaction.” *Ground Engineering* 31(9): 30-33.

Rayamajhi, D., Boulanger, R.W., Ashford, S.A., and Elgamal, A. 2010. “Dense grandular columns in liquefiable ground. II: Effects on deformations.” J. Geotechnical and Geoenviron. Engrg., ASCE, 142(7): 04016024.

Regione Emilia-Romagna, Servizio Geologico Sismico e dei Suoli, ENI-AGIP (1998). Riserve idriche sotterranee della Regione Emilia-Romagna, scala 1:250.000, Bologna (in Italian).

Robertson, P.K. and Wride, C.E. 1998. “Evaluating cyclic liquefaction potential using the cone penetration test.: *Canadian Geotechnical Journal* 35(3): 442-459.

Rollins, K.M., Gerber, T.M., Lane, J.D. and Ashford. S.A. 2005. “Lateral Resistance of a Full-Scale Pile Group in Liquefied Sand.” *J. Geotechnical and Geoenvironmental Engrg.*, ASCE, 131(1) 115-125.

Rollins, K.M., Goughnour, R.R., Anderson J.K.S. and McCain, A. (2004). “Liquefaction hazard mitigation using vertical composite drains.” Procs. 13th World Conf. on earthquake Engineering, EERI, https://doi.org/10.1061/(ASCE)1090-0241(2005)131:1(115).

Rollins, K.M., Quimby, M., Johnson, S.R., Price, B., 2009. “Effectiveness of stone columns for liquefaction mitigation of silty sands with and without wick drains.” U.S.-China Workshop on Ground Improvement, ASCE,

Rollins, K.M., Wright, A., Sjoblom, D., White, N., Lange, C. 2012. “Evaluation of liquefaction mitigation with stone columns in interbedded silts and sands.” In, *Proc. 4th Intl. Conf. on Geotechnical and Geophysical Site Characterization*, Taylor and Francis Group, London, Vol. 2, p. 1469-1475.

Saito, A. 1977. “Characteristics of penetration resistance of a reclaimed sandy deposit and their changes through vibratory compaction.” *Soils and Foundations* 17(4), 31-43.

Saftner, D.A., Zheng, J., Green, R.A., Hryciw, R. & Wissmann, K. 2018. Rammed aggregate pier installation effect on soil properties. *Institution of Civil Engineers-Ground Improvement; Proc.* 171(2): 63-73. London: ICE Publishing.

Seed, H.B. 1987. "Design problems in soil liquefaction." J. Geotechnical Engrg., ASCE, 113(8), p. 827-845.

Seed, H.B. and Idriss, I.M. 1982. "Ground motions and soil liquefaction during earthquakes," Monograph Series, EERI. 130 p.

Smith, M. and Wissmann, K. 2018. "Ground improvement reinforcement mechanisms determined for the M_w 7.8 Muisne, Ecuador, Earthquake." *Geotechnical Earthquake Engineering and Soil Dynamics V*, June 10-13.

Stucchi, M., Meletti, C., Montaldo, V., Crowley, H., Calvi, G.M. and Boschi, E. (2011). Seismic Hazard Assessment (2003- 2009) for the Italian Building Code. Bull. Seismol. Soc. Am., 101:1885-1911; doi:10.1785/0120100130.

Studer, J. and Kok, L. 1980. "Blast-induced excess porewater pressure and liquefaction; experience and application." In *Proc., International Symposium on Soils Under Cyclic and Transient Loading*, 581-593. Swansea, U.K.

Tokimatsu, K., Yoshimi, Y. 1983. "Empirical Correlation of Soil Liquefaction Based on SPT N-Value and Fines Content." *Soils and Foundations*, 23(4): 56-74. https://doi.org/10.3208/sandf1972.23.4_56

van Ballegooy, S., Malan, P., Lacrosse, V., Jacka, M.E., Cubrinovski, M., Bray, J.D., O'Rourke, T.D., Crawford, S.A. & Cowan, H. 2014. Assessment of Liquefaction-Induced Land Damage for Residential Christchurch. *Earthquake Spectra*, 30(1): 31-55.

Vautherin, E., Lambert, C., Barry-Macaulay, D., and Smith, M., 2017, "Performance of Rammed Aggregate Piers as a Soil Densification Method in Sandy and Silty Soils: Experience from the Christchurch Rebuild," In *Proc., 3rd International Conference on Performance-based Design in*

Earthquake Geotechnical Engineering - PBD-III, Vancouver, British Columbia, Canada, July 16-19, 2017.

Vesic, A.S. 1977. "Design of Pile Foundations." Synthesis of Highway Practice No. 42. National Cooperative Highway Research Program, Transportation Research Board, National Research Council, Washington, D.C.

Weaver, T., Ashford, S., Rollins, K.M. 2004. "Performance and Analysis of a Laterally Loaded Pile in Stone Column Improved Ground." In *Proc. ,13th World Conference on Earthquake Engineering,* Vancouver, British Columbia, 1-6 August 2004.

Wentz, F.J., van Ballegooy, S., Rollins, K.M., Ashford, S.A., and Olsen, M.J. 2015. "Large Scale Testing of Shallow Ground Improvements using Blast-Induced Liquefaction." In *Proc., 6th International Conference on Earthquake Geotechnical Engineering - 6ICEGE. Intern. Conf.,* Christchurch, New Zealand, 1-4 November 2015.

Whitman, R.V. 1985. "On liquefaction." Procs. 11th Intl. Conf. on Soil Mech. and Foundation Engrg.

White D.J., M.T. Suleiman, H.T. Pham, and J. Bigelow (2002) "Constitutive equations for aggregates used in Geopier® Foundation Construction", Iowa State University, Civil & Construction Engineering Dept.

Wissmann, K.J., van Ballegooy, S., Metcalfe, B.C., Dismuke, J.N., Anderson, C.K. 2015. "Rammed aggregate pier ground improvement as liquefaction method in sandy and silty soils." In *Proc., 6th International Conference on Earthquake Geotechnical Engineering - 6ICEGE. Intern. Conf.,* Christchurch, New Zealand, 1-4 November 2015.

Wissmann, K.J., Moser, K., Pando, M. 2001. "Reducing Settlement Risks in Residual Piedmont Soils Using Rammed Aggregate Pier Elements." In *Proc., ASCE Specialty Conf.*, Blacksburg, Virginia, 9-13 June 2001.

Zhang, G., Robertson, P.K., Brachman, R.W.I. 2002. "Estimating liquefaction-induced ground settlements from CPT for level ground." *Canadian Geotechnical Journal*, 39(5):1168-1180. https://doi.org/ 10.1139/t02-047

836